AIP | Applied Physics Letters

Embedded indium-tin-oxide nanoelectrodes for efficiency and lifetime enhancement of polymer-based solar cells

Peichen Yu, Chia-Hua Chang, Ming-Shin Su, Min-Hsiang Hsu, and Kung-Hwa Wei

Citation: Applied Physics Letters **96**, 153307 (2010); doi: 10.1063/1.3395395
View online: http://dx.doi.org/10.1063/1.3395395
View Table of Contents: http://scitation.aip.org/content/aip/journal/apl/96/15?ver=pdfcov
Published by the AIP Publishing

Embedded indium-tin-oxide nanoelectrodes for efficiency and lifetime enhancement of polymer-based solar cells

Peichen Yu,[1,a)] Chia-Hua Chang,[1] Ming-Shin Su,[2] Min-Hsiang Hsu,[1] and Kung-Hwa Wei[2,b)]
[1]*Department of Photonics, Institute of Electro-Optical Engineering, National Chiao Tung University, Hsinchu 30010, Taiwan*
[2]*Department of Material Science and Engineering, National Chiao Tung University, Hsinchu 30010, Taiwan*

(Received 26 January 2010; accepted 23 March 2010; published online 16 April 2010)

In this paper, distinctive indium-tin-oxide (ITO) nanorods are employed to serve as buried electrodes for polymer-based solar cells. The embedded nanoelectrodes allow three-dimensional conducting pathways for low-mobility holes, offering a highly scaffolded cell architecture in addition to bulk heterojunctions. As a result, the power conversion efficiency of a polymer cell with ITO nanoelectrodes is increased to about 3.4% and 4.4% under one-sun and five-sun illumination conditions, respectively, representing an enhancement factor of up to ~10% and 36% compared to a conventional counterpart. Also, the corresponding device lifetime is prolonged twice as much to about 110 min under five-sun illumination. © *2010 American Institute of Physics*. [doi:10.1063/1.3395395]

Worldwide awareness of petroleum scarcity and global climate changes has promoted an increasing demand for clean and renewable energy sources, pushing forward the realization of third-generation solar cells.[1] Assisted by simplistic and scalable fabrication processes, organic solar cells have recently emerged as a competitive alternative to their silicon thin-film counterparts. In particular, the power conversion efficiency (PCE) of polymer-based solar cells has recently exceeded 5% due to the introduction of bulk heterojunctions (BHJs).[2–5] However, due to the disordered nature of BHJs, carrier transport remains an issue that limits the PCE from reaching the predicted value of 10%.[6–8] Although recent advances in nanofabrication technologies have allowed the formation of ordered BHJs, offering bicontinuous, interdigitated networks for carrier transport,[9–11] the nanoscale templates still result in limited PCEs, possibly due to insufficient infiltration of polymers or twisted polymer chains that may affect the carrier mobility.[12,13] Here, we introduce an alternative cell architecture which alleviates the transport issue by using embedded indium tin oxide (ITO) nanoelectrodes in polymer-based solar cells. In this architecture, the distributed nanorod electrodes are vertically aligned and protruded into the active layers, offering three-dimensional (3D) conducting pathways for low-mobility holes. Conductive atomic force microscopy (AFM) analyses have shown that the current conduction is significantly improved with nanorod electrodes. As a result, the PCE of a cell with ITO nanoelectrodes is increased to about 3.4% and 4.4% under one-sun (1×) and five-sun (5×) illumination conditions, respectively, representing an enhancement factor of up to ~10% and 36% compared to a conventional counterpart. Also, the corresponding device lifetime, as measured by the degradation time to 80% of the normalized efficiency, is increased twofold to about 110 min under five-sun illumination. The significant efficiency and lifetime enhancements result from the much improved carrier collection probability under high carrier concentrations, suggesting the soundness of the approach toward improving the survivability of polymer-based solar cells.

Although the concept of buried electrodes has previously been proposed to increase cell thickness for optical absorption without compromising charge carrier collection, polymer solar cells with submicroscale lamellar electrodes are still rather inefficient due to the lack of suitable electrode materials and challenging fabrication procedures.[14] In this work, we demonstrate a deposition technique to form free-standing ITO nanorods which is compatible with the standard fabrication process of polymer cells. Figure 1 shows the schematic of a fabricated device with embedded nanoelectrodes. In this cell structure, the randomly oriented nanorod electrodes were deposited on an ITO-coated glass substrate using an oblique electron-beam evaporation method.[15,16] A hole transport layer of poly(3,4-ethylenedioxythiophene)-polystyrene sulfonate (PEDOT:PSS) was then spin-cast onto the ITO electrodes as the anode. The active region consisted of a mixture of regioregular poly(3-hexylthiophene) (P3HT) and [6,6]-phenyl-C60-butyric acid methyl ester (PCBM) with a weight ratio of 1:1. The device was then annealed at 120 °C for 30 min, followed by the thermal evaporation of a 100 nm thick Al electrode. The resulting active-layer thicknesses were ~150–200 nm. A conventional P3HT/PCBM cell with an ITO film electrode was also fabricated with the same process conditions for reference.

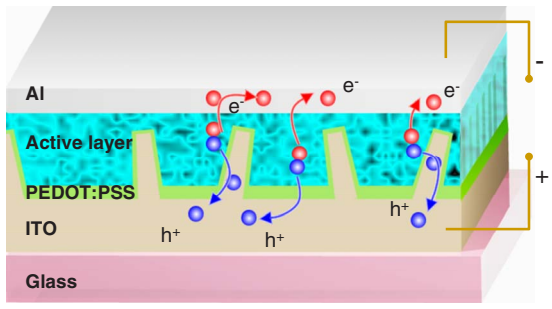

FIG. 1. (Color online) Device schematic with embedded nanoelectrodes. The randomly oriented nanorod electrodes were deposited on an ITO-coated glass substrate using an oblique electron-beam evaporation method, offering 3D conducting pathways for low-mobility holes.

a)Electronic mail: yup@faculty.nctu.edu.tw.
b)Electronic mail: khwei@mail.nctu.edu.tw.

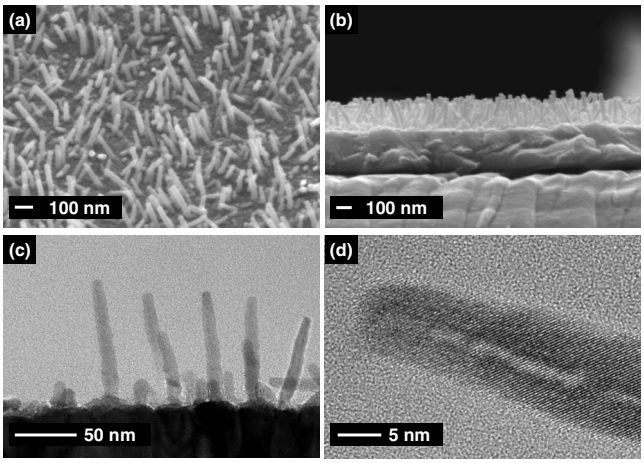

FIG. 2. SEMs and transmission electron micrographs of deposited ITO nanorods on an ITO glass substrate. (a) tilted top view, and (b) cross-sectional view of free-standing nanorods, where the orientations are fairly random; (c) the spacing between rods is on the order of tens of nanometers, sufficient for the infiltration of active materials and (d) the initial formation of a core-shell structure for a single ITO nanorod.

The oblique electron-beam evaporation technique has been used to prepare microscale and nanoscale porous materials based on nucleation formation and self-shadowing effects.[17–19] Although various techniques have been proposed to grow ITO nanostructures, few have actually resulted in free-standing nanorods with high-aspect ratios.[20–22] In this work, a small nitrogen flow rate is introduced to facilitate the segregation of tin-doped indium during nucleation, which promotes the resulting column growth in an oxygen-deficient environment. The scanning electron micrographs (SEMs) for a tilted top view and the cross-sectional view of deposited nanorods are shown in Figs. 2(a) and 2(b), respectively. The deposited nanorods are randomly oriented with heights of ~100 to 150 nm and thicknesses of ~15 to 30 nm. The density can vary from 5×10^9 to 2×10^{10} cm^{-2}, depending on the deposition rate and temperature. These nanorods can be grown in a single-step deposition, up to an area of 3×3 cm^2. As seen in Fig. 2(c), the transmission electron microscopic (TEM) image indicates that the spacing between rods is on the order of tens of nanometers, which is sufficient for the infiltration of the spin-cast active materials. The TEM image of a single rod, shown in Fig. 2(d), further reveals a composition variation in the transverse direction. Our previous work has confirmed the core-shell structure observed in a relatively thick ITO nanorod, where the structure of the outer shell is relatively amorphous due to a higher tin content than that in the core region. The structure in Fig. 2(d) suggests the initial stage of crystallization toward the rod center. The growth mechanism presumably involves self-catalyst, vapor-liquid-solid phase transitions assisted by the introduced nitrogen. As opposed to conventional growths of ITO in an oxygen-rich environment, nitrogen facilitates the segregation of tin-doped indium during nucleation due to oxygen deficiency. The increased tin content then lowers the melting point of tin-doped indium. As a result, when the substrate temperature becomes higher than the melting point of tin-doped indium, the liquid-phase nucleation cores have a large accommodation coefficient to promote the absorption of indium-oxide and tin-oxide vapors via surface diffusion. This process can lead to high growth rates in specific directions, resulting in randomly oriented nanorods.

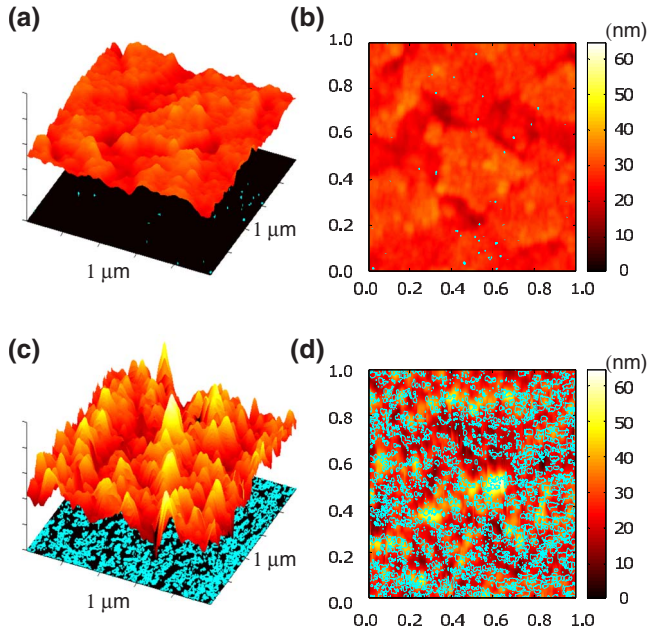

FIG. 3. (Color online) Surface topology and the corresponding current distribution for an ITO film and nanorod electrodes. (a) The measured height image and projected current distribution of an ITO film electrode on a glass substrate; (b) the corresponding 2D topology overlaid with the map of isocurrent contours at a threshold of 34.1 nA; (c) and (d) are the same as (a) and (b), respectively.

The optical transmittance spectroscopy of ITO nanorods deposited on an ITO glass substrate shows a 10–20 nm wavelength shift in the peak transmittance without degradation in magnitudes compared to that of an ITO glass substrate.[23] The contribution to the enhanced optical absorption due to slight differences in the transmittance spectrum is therefore negligible. Since cell characteristics may be primarily determined by electrically-related effects, conductive AFM is employed to study the nanoscale topology and the corresponding current distribution. The measured height image and projected current distribution of an ITO glass substrate scanned within an area of 1×1 μm^2 are shown in Fig. 3(a). In Fig. 3(b), the two-dimensional (2D) topology is overlaid with a map of iso-current contours at a threshold of 34.1 nA. The results for the deposited nanorods on an ITO glass substrate are shown in Figs. 3(c) and 3(d), where the maximum conduction current is as high as 113.7 nA. Since the area scan is performed at a fixed voltage of 10 mV for both samples, the dense and uniformly distributed current spots shown in Fig. 3(d) confirm a conductivity improvement with nanorod electrodes. Moreover, the current distribution is particularly concentrated around the nanorod tips, suggesting a relatively high carrier collection probability near the tips. Such embedded electrodes allow distributed conducting pathways for low-mobility holes, offering a highly-scaffolded cell architecture, in addition to BHJs, for organic photovoltaic devices. The inhomogeneous drift-field distribution in this device may arguably contribute to the germinate separation compared to conventional BHJ cells, which requires further investigation.

Solar cells with embedded ITO nanoelectrodes were characterized under ambient conditions with standard illumination intensities of air mass 1.5, 100 mW cm^{-2} (one-sun, 1×) and 500 mW cm^{-2} (five-sun, 5×), and also compared to conventional cells fabricated with the same process conditions. Hereafter, we refer to the cell with nanorod elec-

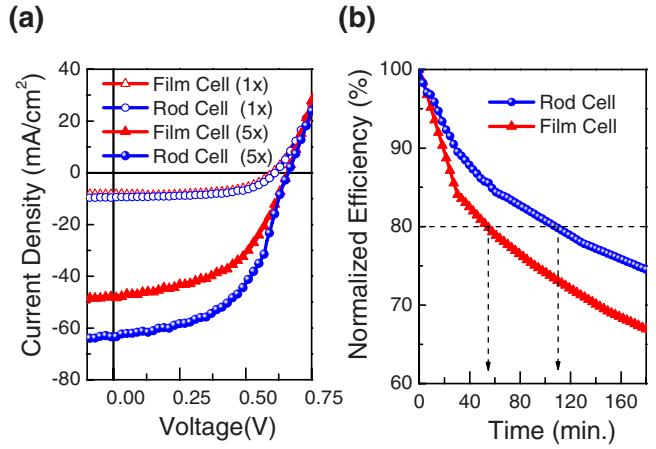

FIG. 4. (Color online) Measured current-density-voltage and lifetime characteristics for a rod cell and a film cell. (a) The power conversion efficiency of the rod cell is increased to about 3.4% and 4.4% under one-sun and five-sun illumination intensities, respectively. (b) The measured lifetime characteristics under a 5× concentration at ambient conditions.

trodes as the rod cell, and the one with an ITO film electrode as the film cell. The measured current density-voltage (J-V) characteristics are plotted in Fig. 4(a) for one-sun and five-sun conditions with the corresponding cell characteristics summarized in Table I. The series and shunt resistance are calculated as the inverse slopes at the open-circuit and short-circuit operation points, respectively.[24] As shown in Table I, the one-sun photocurrent of the rod cell increases by ~14%, compared to that of the film cell. Since the transmittance and cell thickness does not change significantly with the use of embedded electrodes and the series resistance decreases by ~38%, the enhancement of photocurrent and the reduced series resistance are attributed to the improved carrier collection probability using embedded nanoelectrodes. The fill-factor (FF) of the rod cell deteriorates a bit due to a slight degradation of the shunt resistance, possibly originating from a few nanoelectrodes in near contact with the Al cathode. Although not revealed in the preliminary x-ray diffraction analysis, the phase separation of P3HT/PCBM blends may also be affected by nanorod surfaces, which could deteriorate the series and shunt resistance. Overall, the PCE of the rod cell is still enhanced by nearly 10% at one-sun illumination. However, the PCE enhancement becomes prominent with the increased illumination intensity, up to a factor of 36% for the rod cell at a 5× concentration. Since the PCE of both film and rod cells increases with concentration, the enhancement is partly contributed by improved space-charge-limited conduction. Since most of the trap states are occupied due to increased carrier densities under high illumination, the mobility of free carriers increases. However, such contribution should be rather minor as the PCE of the film cell merely increases by 4%. Therefore, we are convinced that the embedded nanoelectrodes can collect holes much more efficiently than the film electrodes under high carrier densities, giving rise to a higher PCE enhancement. Both film and rod cells show decreased FFs due to the increased recombination current under high carrier densities, which are also evidenced by the decreased shunt resistance at a 5× concentration. Finally, the lifetime test was performed for both cells at ambient conditions. As shown in Fig. 4(b), the degradation time to 80% of the normalized efficiency for the rod cell is prolonged twice as much to about 110 min, compared to 55 min for the film cell. The enhanced lifetime of the rod cell may be attributed to the fast collection of charge carriers, which alleviates the impact of charge accumulation on the electrode interface.[25]

TABLE I. Cell characteristics under one-sun and five-sun illumination intensities.

Device (suns)	J_{sc} (mA/cm^2)	V_{oc} (V)	FF (%)	PCE (%)	R_s (Ω cm^2)	R_{sh} (Ω cm^2)
Film cell (1×)	8.35	0.60	62.13	3.11	10.3	250.0
Rod cell (1×)	9.53	0.61	58.70	3.41	6.4	212.2
Film cell (5×)	48.08	0.66	50.99	3.24	4.5	66.0
Rod cell (5×)	67.88	0.66	49.30	4.41	4.0	49.6

The authors thank Professor H. C. Kuo at National Chiao Tung University in Taiwan for technical support and Professor X. Cheng at Texas A&M University, Texas, USA for fruitful discussions. This work is funded by National Science Council in Taiwan under Grant Nos. 96-2221-E-009-095-MY3 and 97-2120-M-006-009.

[1]M. A. Green, *Third Generation Photovoltaics: Advanced Solar Electricity Generation* (Springer, Berlin, 2003).
[2]J. J. M. Halls, C. A. Walsh, N. C. Greenham, E. A. Marseglia, R. H. Friend, S. C. Moratti, and A. B. Holmes, Nature (London) **376**, 498 (1995).
[3]W. Ma, C. Yang, X. Gong, K. Lee, and A. J. Heeger, Adv. Funct. Mater. **15**, 1617 (2005).
[4]M. Reyes-Reyes, K. Kim, J. Dewald, R. López-sandoval, A. Avadhanula, S. Curran, and D. L. Carroll, Org. Lett. **7**, 5749 (2005).
[5]J. Y. Kim, S. H. Kim, H. H. Lee, K. Lee, W. Ma, X. Gong, and A. J. Heeger, Adv. Mater. **18**, 572 (2006).
[6]K. M. Coakley and M. D. McGehee, Chem. Mater. **16**, 4533 (2004).
[7]M. C. Scharber, D. Mühlbacher, M. Koppe, P. Denk, C. Waldauf, A. J. Heeger, and C. J. Brabec, Adv. Mater. **18**, 789 (2006).
[8]W. Shockley and H. J. Queisser, J. Appl. Phys. **32**, 510 (1961).
[9]M. Aryal, F. Buyukserin, K. Mielczarek, X. M. Zhao, J. Gao, A. Zakhidov, and W. Hu, J. Vac. Sci. Technol. B **26**, 2562 (2008).
[10]C. Goh, K. M. Coakley, and M. D. McGehee, Nano Lett. **5**, 1545 (2005).
[11]H. S. Wang, L. H. Lin, S. Y. Chen, Y. L. Wang, and K. H. Wei, Nanotechnology **20**, 075201 (2009).
[12]A. C. Mayer, S. R. Scully, B. E. Hardin, M. W. Rowell, and M. D. McGehee, Mater. Today **10**, 28 (2007).
[13]T. W. Zeng, Y. Y. Lin, H. H. Lo, C. W. Chen, C. H. Chen, S. C. Liou, H. Y. Huang, and W. F. Su, Nanotechnology **17**, 5387 (2006).
[14]M. Niggemann, M. Glatthaar, A. Gombert, A. Hinsch, and V. Wittwer, Thin Solid Films **451-452**, 619 (2004).
[15]P. Yu, C. H. Chang, C. H. Chiu, C. S. Yang, J. C. Yu, H. C. Kuo, S. H. Hsu, and Y. C. Chang, Adv. Mater. **21**, 1618 (2009).
[16]C. H. Chang, P. Yu, and C. S. Yang, Appl. Phys. Lett. **94**, 051114 (2009).
[17]M. M. Hawkeye and M. J. Brett, J. Vac. Sci. Technol. A **25**, 1317 (2007).
[18]Y. P. Zhao, D. X. Ye, G. C. Wang, and T. M. Lu, Proc. SPIE **5219**, 59 (2003).
[19]J. Q. Xi, M. F. Schubert, J. K. Kim, E. F. Schubert, M. Chen, S.-Y. Lin, W. Liu, and J. A. Smart, Nat. Photonics **1**, 176 (2007).
[20]H. Yumoto, T. Sako, Y. Gotoh, K. Nishiyama, and T. Kaneko, J. Cryst. Growth **203**, 136 (1999).
[21]Q. Wan, Z. T. Song, S. L. Feng, and T. H. Wang, Appl. Phys. Lett. **85**, 4759 (2004).
[22]S. J. Limmer, S. V. Cruz, and G. Z. Cao, Appl. Phys. A: Mater. Sci. Process. **79**, 421 (2004).
[23]See supplementary material at http://dx.doi.org/10.1063/1.3395395 for the spectral transmittance.
[24]M. S. Kim, B. G. Kim, and J. Kim, Appl. Mater. & Interfaces **1**, 1264 (2009).
[25]K. Kawano and C. Adachi, Adv. Funct. Mater. **19**, 3934 (2009).